

Opportunities for Deflection of Asteroid Threats

Warren G. Greczyn¹
SPARTA, Inc., Arlington, VA, 22209

and

David F. Chichka²
The George Washington University, Washington, DC, 20052

[Abstract] The kinematic requirements for deflection of asteroid and comet Earth-impact threats are characterized. Direct solutions of Kepler’s equation are coupled to an Earth gravitational model to determine post-deflection orbital behaviors achievable across a representative threat set that spans the orbital behaviors of non-resonant Potentially Hazardous Asteroids. It is shown that a nominal threat deflection capability of 1 cm/s, applied impulsively, provides considerable threat displacement opportunities across a significant portion of observed hazardous threat orbits; deflections at slightly higher imparted velocities are shown to enable defense against a considerable number of additional threat orbits. It is also shown that the temporal windows within which deflections must occur are comfortably long, and that the directional accuracy demanded is not stressing. The “Gravity Tractor” concept is evaluated with respect to its capability against non-resonant threat objects, and it is shown that extending the Tractor concept’s time of action to take advantage of the long temporal windows available for engagements can greatly reduce required spacecraft mass.

Nomenclature

AU	=	astronomical unit – mean distance from the Earth to the Sun
R	=	sphere of influence radius
m_{Earth}	=	mass of the Earth
m_{Sun}	=	mass of the Sun
t	=	time at epoch or other orbital event
a	=	semi-major axis
μ_{Sun}	=	Sun’s gravitational parameter
E	=	eccentric anomaly
e	=	eccentricity
rp	=	perihelion radius
i	=	inclination

I. Introduction

If in the very near future it becomes necessary to attempt the deflection of an Earth-bound asteroid threat, the amount by which we can expect to be able to alter the object’s velocity will be modest at best. However, it can be shown that a simple impulsive deflection of moderate magnitude is sufficient to prevent Earth impact for threats on a wide range of potential impact orbits. It can also be shown that other key metrics of those deflection events are favorable to the defense.

This paper describes the use of direct solutions of Kepler’s equation coupled with Earth gravitational and orbital-motion models to determine post-deflection heliocentric and Earth-relative behaviors of asteroid threats. A parametric representative threat set was developed that spans the orbital behaviors observed in many Potentially

¹ Principal Engineer, 1911 N. Ft. Myer Drive, Suite 1100, Senior Member, AIAA.

² Assistant Professor, Department of Mechanical and Aerospace Engineering, T726, 801 22nd Street NW, Senior Member, AIAA.

Hazardous Asteroids (PHAs; those that can pass within 0.05 AU of the Earth).¹ These are objects that are specifically “non-resonant” in that they are assumed to move directly from the point of engagement to Earth impact without any additional gravitational encounters to perturb their heliocentric orbits. Sample threats were developed at select points within this reference threat, and discrete threat orbits were designed to impact the Earth dead center. A nominal 1-cm/s threat velocity change was applied impulsively at a variety of times prior to Earth impact, with time of deflection incremented backwards until a full 10 threat orbits before Earth impact. For each deflection time, threat displacement at closest passage to Earth was calculated by accounting for heliocentric motion of the deflected threat, heliocentric motion of Earth, and geocentric threat motion once inside of the Earth’s sphere of influence.

The primary product of the described analysis was an estimate of the percentage of expected threat orbits that could be mitigated with the baseline 1-cm/s impulsive velocity change. Other trends key both to judging the potential for successful near-term asteroid threat deflection and to making critical resource decisions in design of planetary defense systems, missions, and programs are presented and discussed, including: the latest possible deflection opportunities; the degree to which additional deflection opportunities can be achieved with increased warning time; the miss-distance margin that can be expected in successful deflections; the degree to which additional deflection opportunities can be achieved for moderate increases in velocity change; the required accuracy of deflection direction and timing precision of the deflection event; and the degree to which threat inclination can be expected affect deflection success.

II. Planetary Defense Representative Threat Set

A representative threat set was developed to enable a parametric analysis across the full span of potential asteroid threat orbits. This threat set encompasses the full range of perihelia, eccentricity, and inclination values observed in PHAs. Sample threats were then selected parametrically throughout this set, with upper and lower bounds and parametric step sizes selected according to the distribution pattern seen in each element. Histograms of these distributions are shown in Figures 1, 2, and 3 for perihelia, eccentricity, and inclination, respectively. (As is standard for histograms, each bin is set so that the “Count” represents the number of occurrences at or below any particular value, down to but not including the next lowest labeled bin value.)

Based on these distributions, bounding values and associated parametric step sizes were selected as shown in Table 1. Note that the step sizes for inclination were set more closely at low values, reflecting the trailing-off of the PHA population at higher inclinations indicated in Figure 3. Perihelia and eccentricity were better behaved; a single step size for each was deemed sufficient.

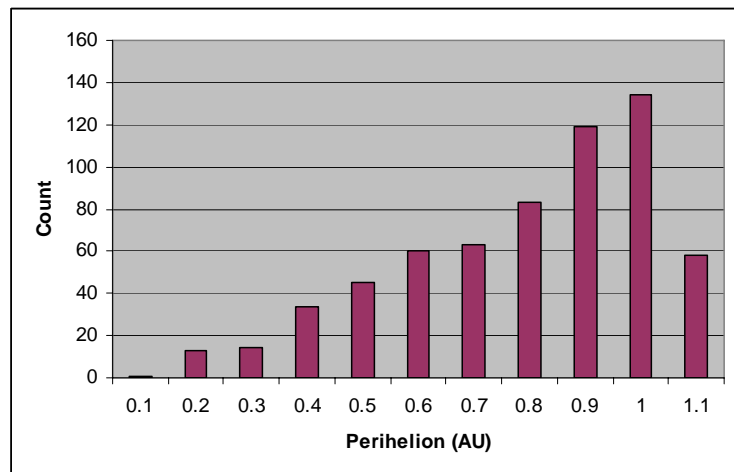


Figure 1. Histogram of Radii of Perihelion for Observed PHAs.

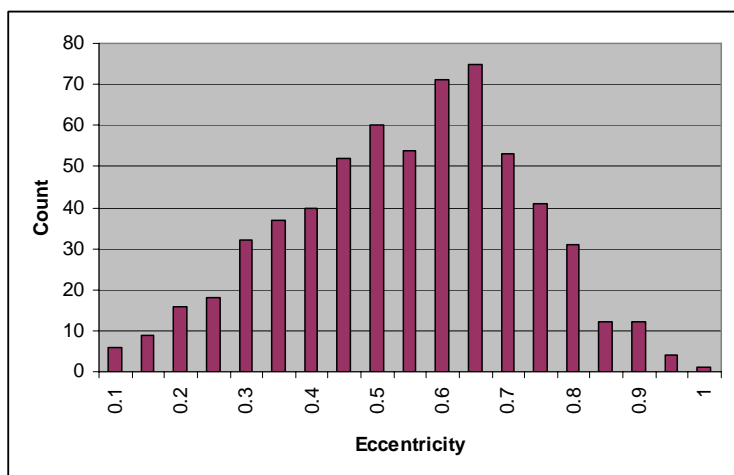


Figure 2. Histogram of Eccentricities for Observed PHAs.

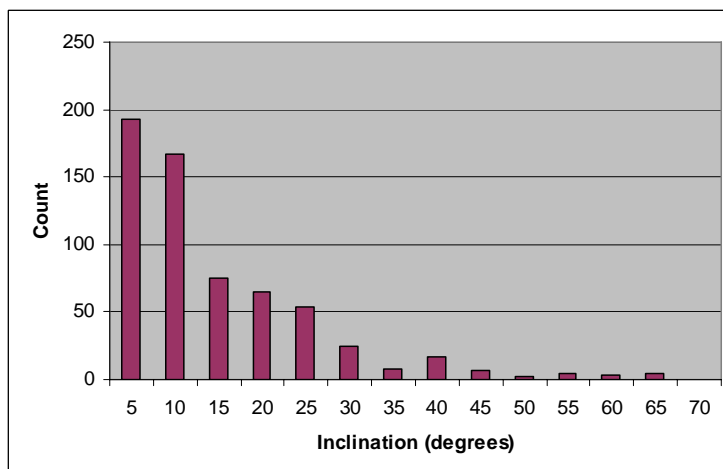


Figure 3. Histogram of Inclinations for Observed PHAs.

Table 1. Parametric Limits of Representative Asteroid Threat Orbits.

Orbital Element	Value Extents	Baseline Step Sizes
Radius of Perihelion	0.1 AU to 1.0 AU	0.1 AU
Eccentricity	0.1 to 0.99	0.1 + 0.99
Inclination	0 degrees to 70 degrees	0, 5, 10, 15, 25, 40, 70

III. Threat Displacement Simulation

The earliest efforts to describe the post-deflection orbits and Earth-relative motions of impulsively-deflected threat objects were strictly linear in nature.² These techniques, extrapolated from circular-orbit solutions, asserted merely that the velocity change to be inflicted on a threat object varied inversely with the amount of time left before that impact. A more complex, non-linear closed-form approach was later developed to estimate near-optimal deflection solutions,³ but it could not be applied more than one orbit prior to impact, and did not account for Earth's gravity or for Earth-to-threat relative motion in the calculation of threat displacement. A subsequent work developed a technique for estimating threat velocity change from engagements occurring more than one threat orbit in advance. This effort did discover some of the finer structure that exists in the deflection data, but Earth gravitational effects were still neglected.⁴

The simulation codes developed for this effort are applicable many threat orbits in advance, account for Earth-to-threat relative motion, and also provide increased accuracy through the modeling of the aforementioned Earth gravitational effects. The Earth-to-Sun gravitational sphere of influence used was that suggested by Laplace and is as shown in Equation 1.⁵

$$R = (AU) \left(\frac{m_{Earth}}{m_{sun}} \right)^{2/5} \quad (1)$$

In this equation, R is the sphere of influence radius, AU is an astronomical unit, the mean distance from the Earth of approximately 150 million kilometers, and the Earth-to-Sun mass ratio is as shown. The resulting Earth-to-Sun sphere of influence has a radius of just under 925,000 kilometers or about two and a third times the Earth-Moon distance.

Multi-orbit heliocentric solutions were attained through iterative numerical solution of Kepler's Equation, shown as Equation 2.⁶

$$t_2 - t_1 = \sqrt{\frac{a^3}{\mu_{Sun}}} [E_2 - E_1 - e(\sin E_2 - \sin E_1)] \quad (2)$$

The left side of this equation is the time from deflection to Earth impact, a is the threat orbit's semi-major axis, μ_{Sun} is the Sun's gravitational parameter (equaling, by definition, the Sun's mass multiplied by the Universal Gravitational Constant), E is the threat orbit's eccentric anomaly at the times of interest, and e is the threat orbit's eccentricity. The Kepler solution itself was carried out by standard Newton iteration.

The simulation began with the selection of parametric values for the three key threat orbital elements of interest: perihelion radius (rp), eccentricity (e), and inclination (i). Orbital modeling proceeded as shown in Figure 4, with placement of the Earth at autumnal equinox, selected because of convenience of sign convention: this point is located at an assumed 1 AU out along the direction of the vernal equinox, which, conveniently, is the positive-X direction of the heliocentric inertial Cartesian coordinate system. (Because threat orbital elements are selected parametrically, no reduction in the applicability of the representative threat set is suffered from ignoring the slight eccentricity of Earth's orbit.)

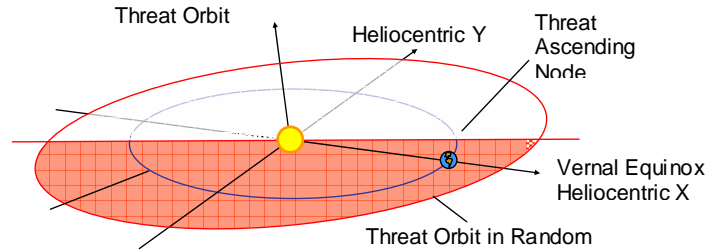


Figure 4. Representation of Process for Generating an Earth-Impact Threat: Step 1.

Next, the standard conic equations were applied to calculate threat semi-major axis and radius of aphelion, with the threat's orbit at this point still in essentially a random orientation. (The shading of the threat orbit indicates the portion that is below the ecliptic.) With the threat orbit size, shape, and tilt determined, the inertial orientation required for Earth impact was then established by rotating the orbit in the heliocentric X-Y plane so as to place ascending node along the direction of vernal equinox, as shown in by Figure 5.

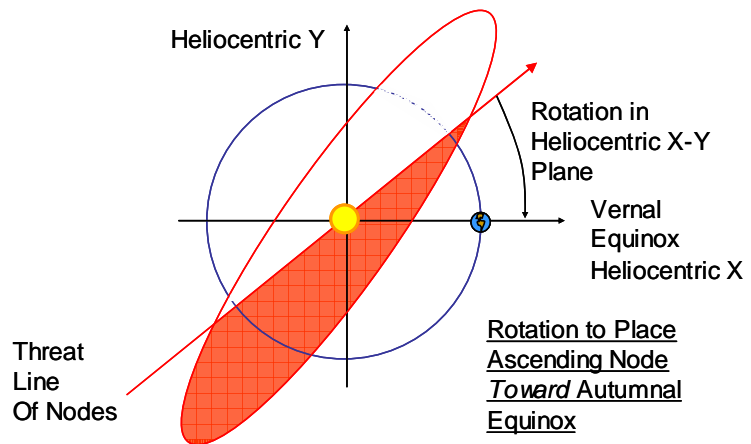


Figure 5. Representation of Process for Generating an Earth-Impact Threat: Step 2.

The threat orbit was next rotated about its own normal axis until the orbit crossed the ecliptic at a range of 1 AU. This was done by zeroing out longitude of ascending node and solving for the value of argument of perihelion that forces threat ecliptic crossing at that desired 1 AU. This final rotation is shown in Figure 6 along with an oblique view of the previous rotation.

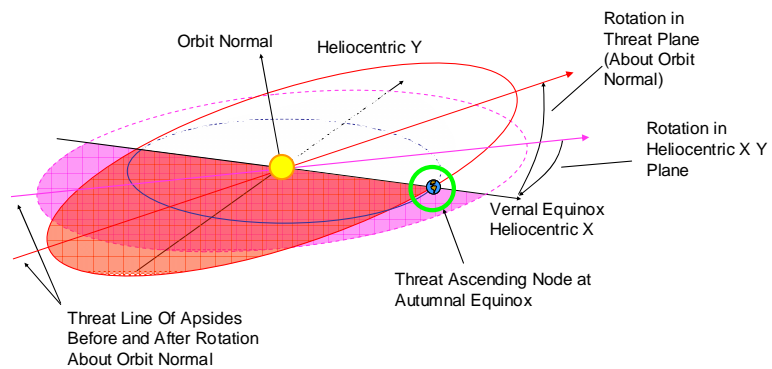


Figure 6. Representation of Process for Generating an Earth-Impact Threat: Step 3.

Having arranged for the centers of both the Earth and the threat object to arrive at autumnal equinox at the same time, the code then simultaneously back propagates both bodies until the threat arrives at the edge of the Earth-to-Sun sphere of influence. The back propagation from impact to the sphere of influence is shown in Figure 7.

The threat is now temporarily frozen at the edge of the sphere of influence. From this point in the analysis, whenever the threat is inside this sphere it moves solely under Earth's gravity, generally along a hyperbolic path in geocentric space. However, the threat velocity vector at its present position on the sphere of influence is still that which was calculated to deliver the threat along an elliptical path in heliocentric space to the equinox simultaneous to the arrival of Earth's center at that same point in space, a path that neglects Earth gravity (the dashed-line in Figure 7 passing through the equinox). The velocity vector that the threat needs to possess is that which places it on a path leading to a dead-on impact under the influence of Earth's gravity only. To make the needed modification, the velocity portion of the state vector is realigned so as to point directly at the Earth's center, thus guaranteeing a "dead-on" hit for continued propagation under the influence of Earth gravity only. This modified path is represented by the dotted line in Figure 8. The actual time of impact is allowed to change slightly to account for a small difference in time of flight between the hyperbolic/geocentric and the elliptical/heliocentric paths from the edge of the sphere of influence. Angular separation of the two vectors has been exaggerated for graphical clarity: actual velocity vector realignments are small in magnitude.

With a dead-on impact now assured, the modified threat state vector is back-propagated along the solid orbit line in Figure 8 to a position designated by a particular deflection time of interest prior to Earth impact. At that point, the code transforms the threat state into threat-local coordinates and applies the desired deflection according to the geometries shown in Figure 9, where the largest and noticeably out-of-scale vector represents the desired, user-selected velocity increment that is to be added to the threat's instantaneous velocity.

The direction in which the velocity change is to be imparted is described by two independent angles that are measured relative to the threat's heliocentric position and velocity vectors. The first angle, termed the "Transangle," is the measure between the imparted velocity vector and the plane normal to the threat's instantaneous orbital velocity vector, making it essentially a local elevation angle of the imparted velocity. As with topographic elevations, Transangle can possess values between positive and negative 90 degrees. The second angle, termed "Planeangle," is measured between the threat's orbital radial direction and the projection that the applied velocity makes onto the normal plane previously described. This construction makes Planeangle essentially an azimuth measure, its datum being the threat-local coordinate axis lying in the orbital plane, and its values ranging between positive and negative 180 degrees. While this construction allows the imparted velocity change to be applied in any desired direction, deflection components out of the threat orbital plane in general did not add significantly to the attainable threat displacement, and therefore were not included in the main analysis.

With the threat's velocity now modified as desired, the code transforms the threat's state from local coordinates back to heliocentric coordinates, and then forward propagates the threat along its altered orbit. When the altered inbound threat again approaches the Earth, it is refrozen at the edge of the sphere of influence, and its new

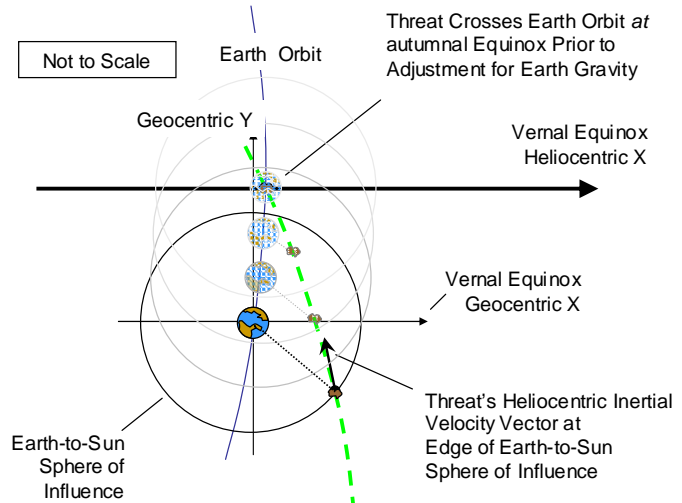


Figure 7. Use of Sphere of Influence in Modifying Pre-Deflection Threat Orbit: Step 1.

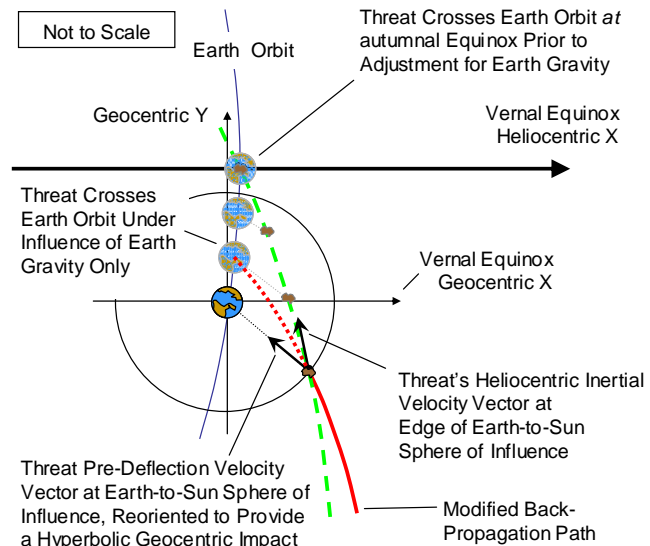


Figure 8. Use of Sphere of Influence in Modifying Pre-Deflection Threat Orbit: Step 2.

heliocentric inertial state vectors are translated into geocentric inertial coordinates, making the orbit again hyperbolic/geocentric in nature. Finally, threat displacement in the form of closest passage between the center of the Earth and that of the threat is calculated as a hyperbolic miss distance. These last two steps are depicted in Figure 10.

The modeling process itself was implemented by way of a series of linked MATLAB codes that, for each incremented time of engagement, performs the back propagation, deflection, forward/re-propagation, and, finally, calculation of the threat displacement at closest hyperbolic Earth passage. This calculation string was executed at each engagement time for a span of deflection directions, all in-plane and ranging from being aligned with the threat's orbital velocity to directly opposing it. A control code then collects the displacements achieved at the various Transangle and Planeangle directional settings, searches through them to identify the peak attainable threat displacement, and records it along with its associated engagement time. Each analysis run began at 50 days prior to impact, and then moved back one day at a time to cover just over 10 full threat orbits.

IV. Asteroid Example Case

The post-deflection threat displacement data obtained from the described simulation codes are now introduced by way of a nominal example asteroid with $r_p = 0.7$ AU, $e = 0.4$, and $i = 0$ degrees. Figure 11 plots this threat object as it moves through one orbit over its approximately 460-day period. Note the direction of the threat's orbit as it approaches Earth impact.

Figure 12 shows the principal form of "displacement curve" output obtained from the simulation runs: this is the maximum achievable threat displacement (measured center-to-center with the threat object at closest Earth passage) achievable for a 1-cm/s deflection. (All other cases that follow likewise use a 1 cm/s velocity change unless specifically noted.) The figure shows achievable displacement of the example threat over multiple threat orbits prior to Earth impact; each vertical green line marks the passage of the threat through its perihelion. The data set for Figure 12 was run so as to reach back in time far enough to find a displacement peak that would result in a threat displacement of at least the Earth's radius plus 110 kilometers of substantive atmosphere. This distance of 6488 kilometers, herein assumed to be the minimum displacement required for a "successful" deflection, is marked by a horizontal line. The plot shows that in order to achieve a zero-margin Earth miss against the example threat, the latest that a 1-cm/s deflection can be applied is approximately 6 years, 21 days before Earth impact. Figure 13 shows the deflection directions required to produce these maximum threat displacements. Note the markedly cyclic but

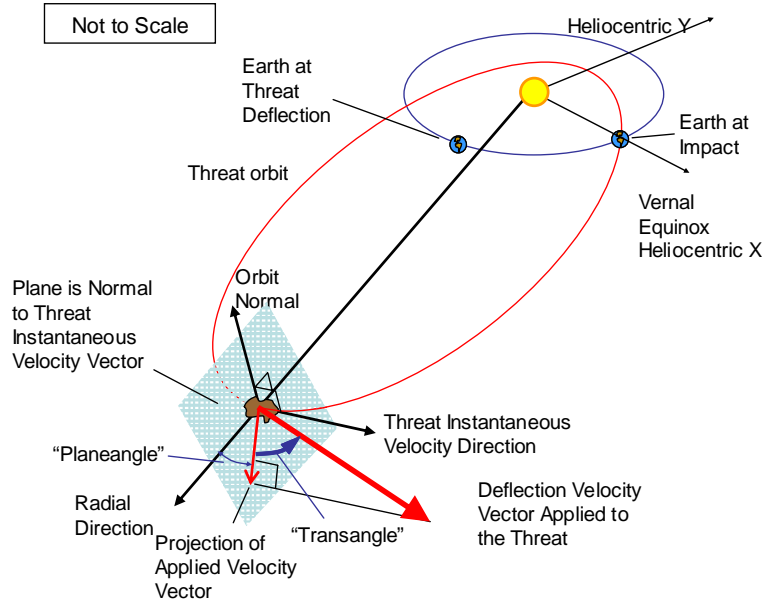


Figure 9. Geometry of Applied Deflection Velocity.

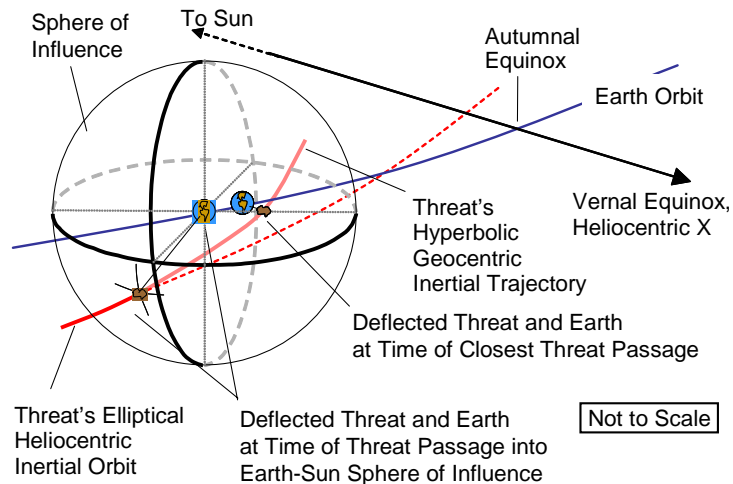


Figure 10. Use of Sphere of Influence in Calculating Threat Displacement at Earth.

convergent behavior. (For a 90-degree Transangle, the imparted velocity change is aligned with the threat velocity vector in accordance with the construction of Figure 9.)

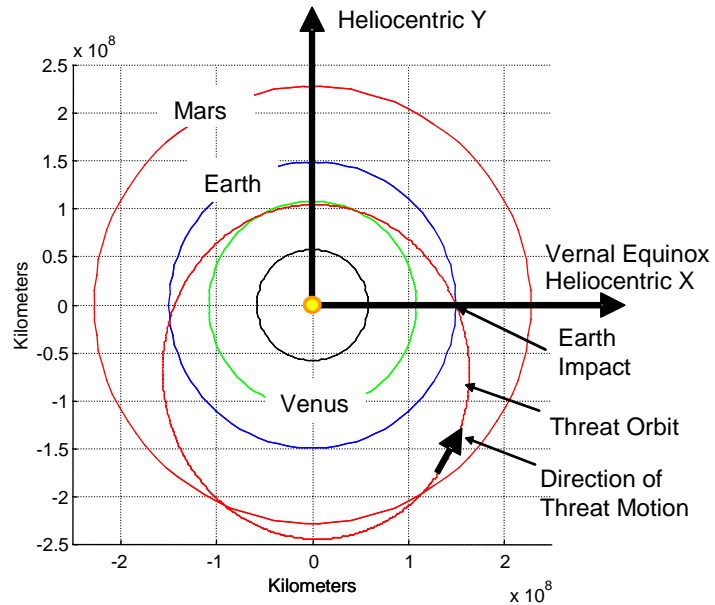


Figure 11. Example Threat Orbit for One Period.

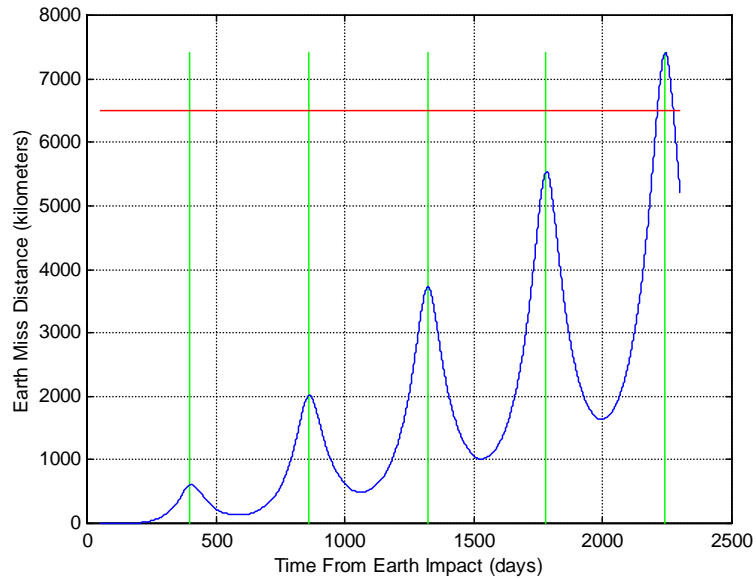


Figure 12. First Successful Mitigation for Example Threat Case.

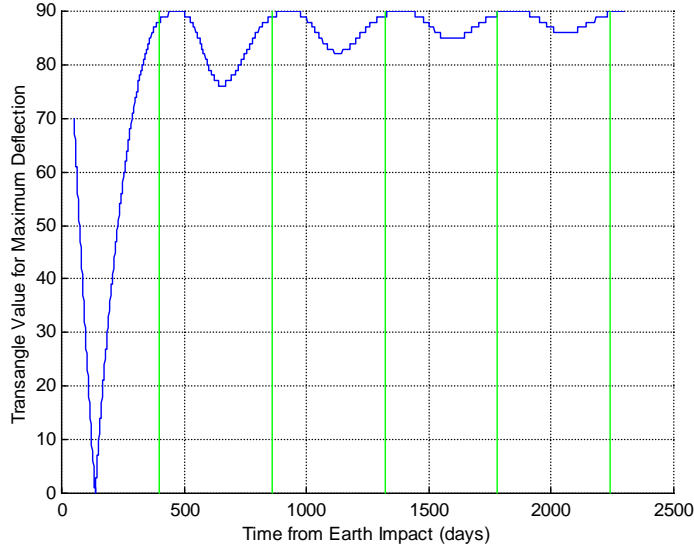


Figure 13. Example Threat Transangle Values for Maximum Threat Displacement.

V. Deflection Opportunities and Characterization

A. Representative Threat Set Analysis Points

Table 2 lists the parametric values of asteroid perihelion and eccentricity that were selected as the representative threat set for this effort. The bulk of the values were developed by matching whole-decimal values of perihelion from Table 1 to a range of eccentricities, also from Table 1 and also in whole-decimal steps. Next, appropriate

Table 2. Parametric Run Case Summary.

Radius of Perihelion r_p (AU)	Eccentricity e	Limit Case Description (if applicable)
0.1	0.846, 0.9, & 0.956	Low: limit on semi-major axis High: limit on eccentricity
0.2	0.7065, 0.8, 0.9, & 0.944	Low: limit for deflection of 1 Earth radius High: limit on aphelion
0.3	0.593, 0.6, 0.7, 0.8, 0.9, & 0.918	
0.4	0.494, 0.5, 0.6, 0.7, 0.8, 0.890	Low: limit for deflection of 1 Earth radius High: limit on semi-major axis
0.5	0.407, 0.5, 0.6, 0.7, 0.8, 0.863	
0.6	0.333, 0.4, 0.5, 0.6, 0.7, 0.8, 0.836	
0.7	0.271, 0.3, 0.4, 0.5, 0.6, 0.7, 0.8, 0.808	
0.8	0.225, 0.3, 0.4, 0.5, 0.6, 0.7, 0.781	
0.9	0.209, 0.3, 0.4, 0.5, 0.6, 0.7, 0.753	
0.99	0.357, 0.4, 0.5, 0.6, 0.7, 0.729	

boundary cases were developed by holding perihelion strictly to its whole-decimal values and then varying eccentricity until the resulting semi-major axis and aphelion matched the values possessed by the extremes of the observed threat. Because the geometric modeling used in the threat displacement calculation code is efficient for threat orbits that are Earth-crossing but not for those that are osculating, the largest perihelion value was set at 0.99 AU instead of the 1.0 AU listed in Table 1. Finally, so as not to expend analysis effort in the evaluation of trends that might apply only to small, unsuccessful threat displacements, low-end limits on eccentricity were established such that at least the 10th deflection peak resulted in an Earth miss.

Each of the perihelion/eccentricity combinations captured in Table 2 was analyzed at inclinations of 0, 5, 10, 15, 25, 40 and 70 degrees, as was stipulated in Table 1. This produces a representative threat set containing 420 discrete threat members made up of 60 perihelion/eccentricity pairings, each evaluated at the 7 discrete inclinations. The core analysis product developed for this paper is a collection of displacement curves like that of Figure 12, calculated for each of these 420 combinations, and each reaching back to a full 10 threat orbits before Earth impact. With those curves each starting at 50 days prior to Earth impact and progressing in 1-day increments, the number of discrete deflection events represented in this analysis totals approximately 630,000.

B. Overall Asteroid Deflection Opportunities

A deflection capability metric of primary interest is the percentage of the representative threat set that can be successfully deflected at the 1-cm/s level. This was calculated as the percentage of the total number of deflection curve peaks (each of which represents the optimal deflection opportunity that occurs once per threat orbit, approximately at threat perihelion) that surpass the Earth-miss threshold depicted in Figure 12 by the horizontal line at 6488 kilometers. In addition, the constraint discussed earlier that eliminated unsuccessful perihelion/eccentricity pairings was temporarily lifted to avoid a bias toward opportunities for successful deflection that would have underrepresented the more challenging portion of the threat. With those unsuccessful cases temporarily added back in, the resulting “unconstrained” set possesses 4760 peak deflection opportunities, made up of 68 perihelion values, 7 inclinations, and 10 peaks per combination. All of these are represented in Figure 14, which shows the relationship of successful to unsuccessful 1-cm/s peak deflection opportunities, grouped by threat perihelion.

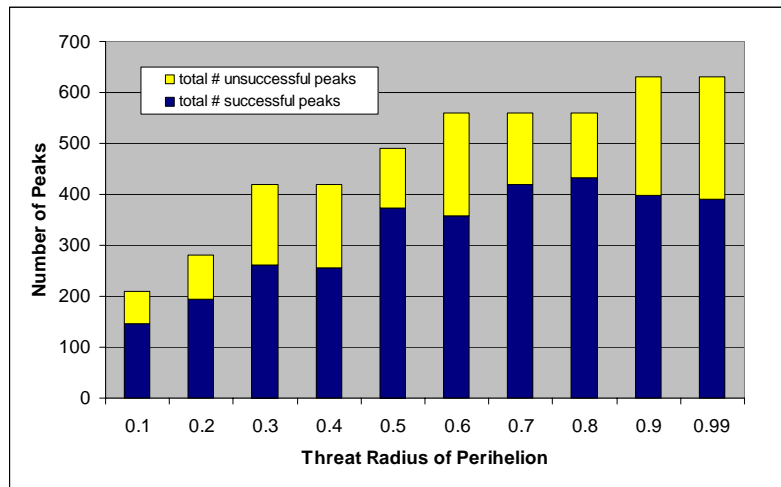


Figure 14. Total and Successful Deflection Peaks by Perihelion for Unconstrained Representative Threat Set.

From this it is found that 68% of peak deflection opportunities at 1 cm/s produce successful Earth misses, indicating that there should be significant opportunities to conduct successful planetary defense even in the near term. Through an extended analysis it was found that if surveillance and prediction allow engagements to take place 20 orbits ahead of Earth impact, nearly 80% of peak opportunities could be successful at 1 cm/s.

C. Latest Possible Asteroid Deflection Before Earth Impact

Another deflection capability metric of particular interest is how soon before an impending Earth impact a nominal deflection can be applied and still achieve an Earth miss. The plot in Figure 15 gives the latest possible times for achieving deflections of zero margin (i.e., deflections of 6488 kilometers, but no more) at 1 cm/s against threats with zero-degree inclination. Note that these data points do not represent “peak” deflection opportunities; instead, they are the first times that each displacement curve rises above the 6488-kilometer “Earth miss” threshold. For graphical clarity, only

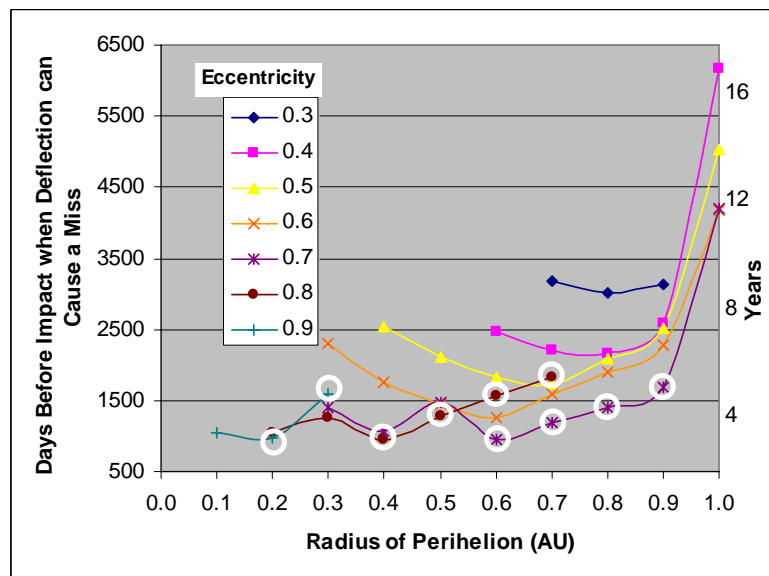


Figure 15. Latest 1 cm/s Earth-Miss Deflection Opportunities.

whole-decimal eccentricity values from Table 2 are presented.

Figure 15 shows that for the conservative deflection level, no successful deflection opportunities exist earlier than about 2.6 years prior to Earth impact, and only one-third of the threat can be successfully deflected if addressed within 5 years of their respective impacts. However, engaging at least 10 years before Earth impact would enable over 93% of these late-deflection opportunities.

The circled points scattered along the bottom of Figure 15 are of particular interest, as they represent those deflection opportunities that occur after the threat's last pre-impact threat perihelion. Clearly not all successful deflection events will have to occur numerous threat orbits in advance. It should be noted, however, that none of the circled data points provide an Earth miss after the threat has passed its last pre-impact aphelion: conservative levels of impulsive deflection do not work when the threat is on its "final approach."

D. Threat Displacement Margin Through Earlier Deflection

In an actual planetary defense engagement, every attempt will be made to maximize threat displacement margin. The general form of the threat displacement curves (as was shown in Figure 12) makes it clear that the earlier an Earth impactor is located and acted on, the greater the achievable margin. Figure 16 was developed by assuming that the default 1-cm/s displacement must produce an Earth miss of a full 10 Earth radii (along with an equal number of 110-kilometer atmosphere thicknesses).

The data indicate that there are a fair number of high-margin deflection opportunities, although many of them demand long lead times (i.e., early threat engagements). Also of note is that there are no high-margin opportunities against threats with eccentricities below 0.6. This is because large margins require time for the threat object displacement to accumulate after deflection, but many of the threats of interest with smaller eccentricities have smaller periods, so there is not enough time to accumulate sufficient displacement within the 10-threat-orbit limit.

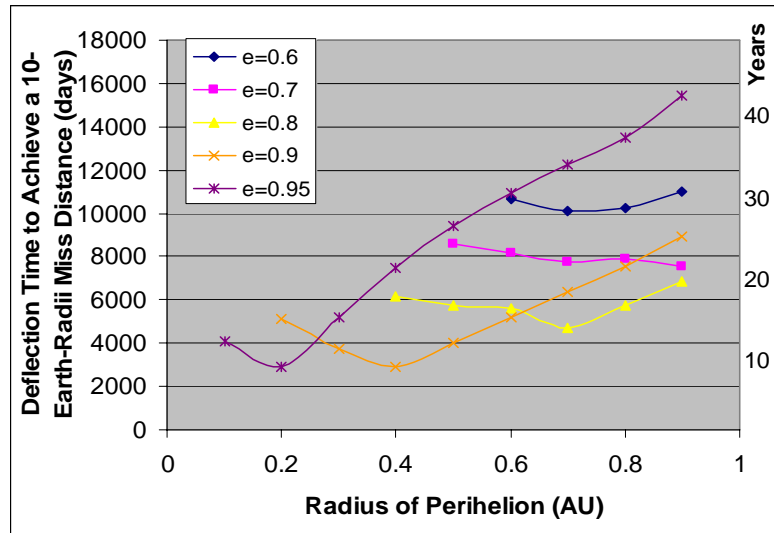


Figure 16. Deflection Times to Achieve Threat Displacement of 10-Earth Radii with a 1 cm/s Deflection.

E. The Effect of Various Imparted Velocity Changes on Displacements

Also of interest is the degree to which we might be motivated to increase our capability to impart a velocity change above 1 cm/s. Figure 17 presents the deflection velocities required to achieve successful zero-margin Earth miss across the representative threat set at the final deflection peak before pending Earth impact. (The cases shown are only those that would *not* have achieved successful Earth miss with only a 1 cm/s deflection.) Note the 1 cm/s threshold indicated by the horizontal line near the bottom of the plot.

The plot shows that taking advantage of all or even most of the described cases would require some fairly extreme deflection velocities, up to 25 cm/s for

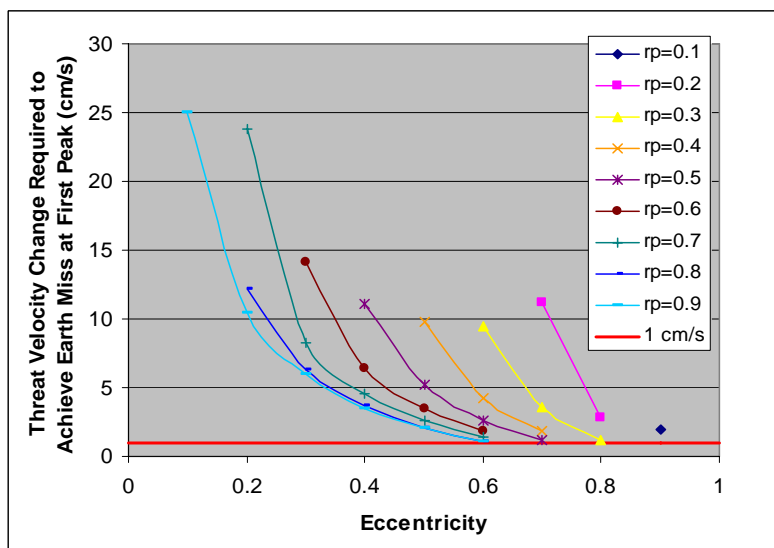


Figure 17. Deflection Velocities Required to Recover a Full Earth Miss.

high-perihelion/low-eccentricity cases. This is because the objects at this end of the scale have periods approaching that of Earth, which, again, often results in an insufficient amount of time for threat deflection to accumulate to that required for an Earth miss. Of critical note, however, is that there exist many last-peak deflection opportunities clustered near the 1-cm/s line, waiting to be taken advantage of should deflection velocities be available that are even slightly above that nominal level. This is more clearly displayed in Figure 18, which presents the cumulative distribution of the imparted velocities contained in Figure 17. Any point on the curve represents the total number of previously unsuccessful last-peak deflections that would become successful at the associated threat deflection velocity.

It is seen that relatively small increases in deflection velocity above the 1-cm/s baseline result in significant increases in the number of successful displacements achievable at the last peak before impact: approximately 25% of the non-available cases are reclaimed with only a 2-cm/s deflection, and 50% of the cases are had for 4 cm/s. There is not significant motivation to go much beyond that, however, as the cumulative distribution begins to lose slope, and serious questions should arise as to whether the kinds of deflection velocities represented by the upper portions of this curve would ever be achievable.

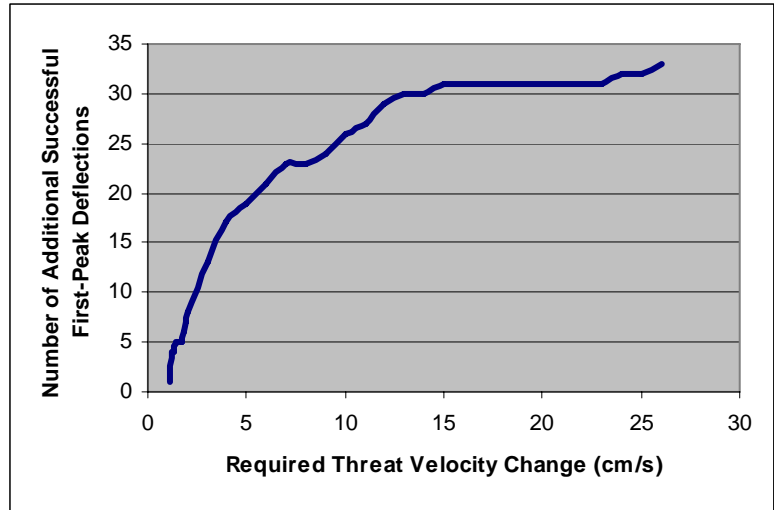


Figure 18. Sorted Distribution of Threat Velocity Change Required to Achieve a True Earth Miss.

F. Angular Deflection Window

Because most if not all of the impulsive deflection techniques make no promises regarding control over the exact direction in which the imparted velocity is applied, the angular accuracy within which we would need to deflect a threat object is of considerable interest. With “angular deflection window” defined as that full-angle measure of the imparted velocity direction within which a deflected threat would achieve at least 90% of the displacement available from an optimally-directed deflection, Figure 19 gives the allowable angular error in deflection direction for a broad sampling of the representative threat set, including threats across the full range of inclinations.

In general, the directional accuracy required of impulsive deflections is seen to be fairly and perhaps even comfortably large across the entirety of the representative threat set, but the unknown nature of threat physical properties and behaviors cannot be ignored. In actuality, the threat’s topography, rotational or tumble dynamics, and internal makeup will most likely not be known to any great degree, producing considerable uncertainties as to the placement of the line of action of a deflection impulse and therefore at least equal uncertainty in the ultimate direction of motion of the deflected object. These factors may well conspire to overtake any advantage that might have been hoped for by way of the data shown in Figure 19.

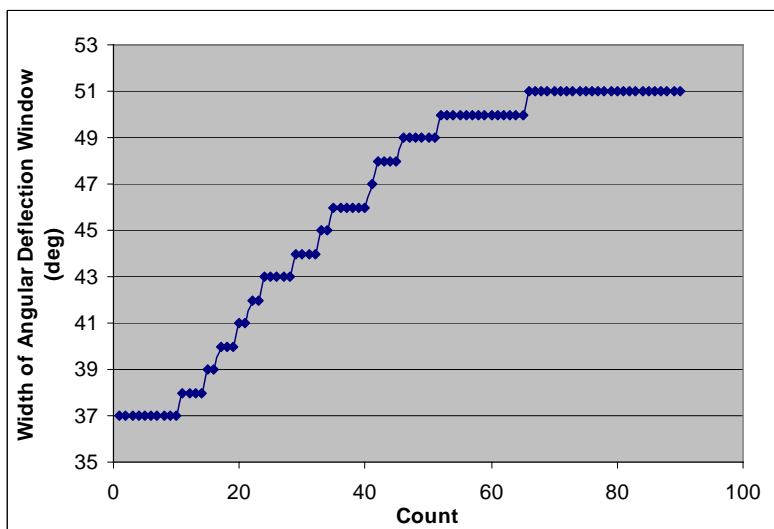


Figure 19. Sorted Distribution of Angular Deflection Window.

G. Deflection Window Duration

To explore the expected size of the temporal window within which we must engage a threat object to assure a sizable Earth miss, deflection window durations were calculated at the first and tenth displacement peaks for threat inclinations of 0, 25, and 70 degrees. Much like the angular window, the “temporal deflection window” will be defined as the span of time over which a threat can be deflected and still result in at least 90% of a threat displacement performed with optimal timing. The main plot of Figure 20 shows the sorted distribution of window durations for both successful deflection attempts (i.e., those achieving a 6488 kilometers displacement) and unsuccessful ones.

There are clearly numerous cases where the deflection window has a very comfortable duration; note that 95% of the threat presents a window of greater than 5 days. The inset shows comparable behavior of the distribution when only successful cases are counted, and compares closely with the more inclusive data set shown in the main plot. This indicates that unsuccessful cases are represented fairly evenly throughout the field.

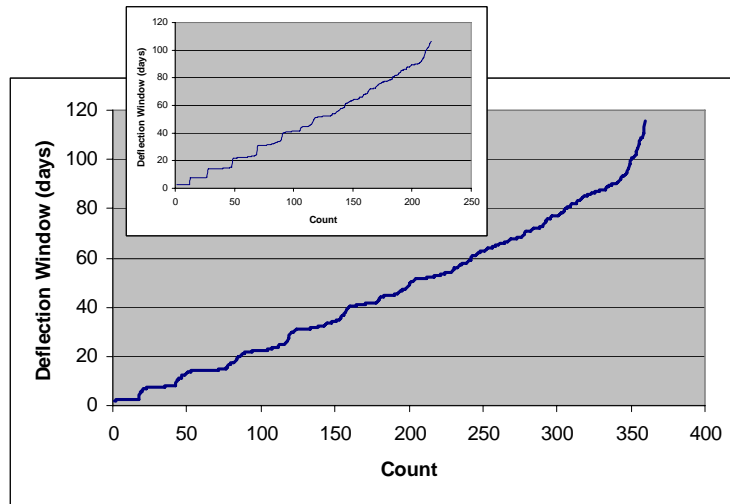


Figure 20. Sorted Distribution of Temporal Deflection Window.

H. Threat Displacement Behavior Over a Range of Threat Inclinations

Much of the data presented thus far have been for zero-degree threat inclination. Because observed threat objects tend toward low inclinations (as was shown in Figure 3) this can be taken as a moderately acceptable supposition, but inclination does have a measurable effect. Figure 21 shows normalized threat displacements for a variety of perihelion/eccentricity combinations, with the normalization point being the magnitude of threat displacement attained at the last deflection peak before Earth impact. The data show that attainable threat displacement for threats with small perihelia and moderate to large eccentricities is relatively unaffected by threat inclination and in fact tails off slightly for the rarer high-inclination asteroid threats. However, for objects with the highest perihelia the effect of inclination becomes quite pronounced and is in our favor. Although its behavior still tails off for 70-degree threats, normalized threat displacement rises dramatically for very large perihelia and low eccentricity.

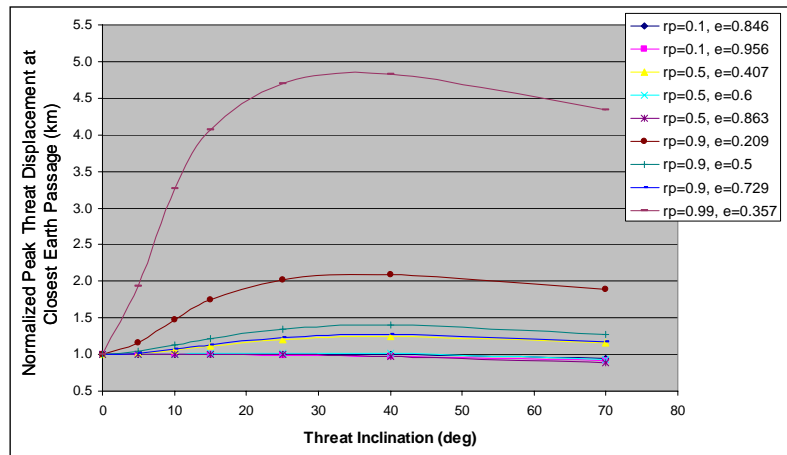


Figure 21. Sorted Distribution of Temporal Deflection Window.

I. Application of the Gravity Tractor

The concept of a Gravity Tractor entails the use of a hovering spacecraft positioned at a small and essentially constant distance above the surface of an asteroid for a period sufficient to allow the mutual gravitational attraction between the two bodies to impart a velocity change to the asteroid. The concept was first introduced in the 10 November 2005 issue of *Nature*, and is further explained in a subsequent white paper titled “Threat Mitigation: The Gravity Tractor.”⁷ That white paper describes the application of this concept against two particular asteroids: 99942 Apophis (2004 MN4), and 2004VD17. For the deflection of Apophis, a Tractor engagement would aim to alter the conditions of an encounter that object will have with Earth in 2029; if not altered, that encounter will be

close enough to cause a subsequent encounter in 2036 to have a small but non-zero probability of resulting in an Earth impact, a behavior indicative of what are termed “resonant return keyhole” orbits. The “keyhole” or corridor through which objects must pass in order for the subsequent encounter to result in an actual Earth impact is quite small. The Gravity Tractor white paper gives the velocity change required to mitigate Apophis as only 2×10^{-6} m/s, or the-tenths of a percent of the 1 cm/s baseline.

The associated mission to Apophis would occur in 2027, and the velocity change would be delivered by way of a spacecraft of only 1 metric ton that maintains a distance of approximately 240 meters from the object’s gravitational center for 20 days. The white paper does not provide the calculation process used to determine the 2×10^{-6} m/s requirement, but it does state that the deflection velocities Apophis, 2004VD17, and other return-resonance-keyhole objects are in general many orders of magnitude smaller than those required for objects that are *non-resonant*, including the more general population of PHAs referenced in the earlier sections of *this* paper that can present an Earth impact threat without any intervening encounters. It also very clearly acknowledges that the extremes of required velocity changes between the two classes of objects (i.e., resonant and non-resonant) make “likely [the] need for deflection concepts of widely ranging capability.” This is not, however, the conclusion found in the popular press, which has described the Gravity Tractor approach as “The favored approach to dealing with a potentially deadly space rock”.⁸ It is hoped that the quantifications given below will allow this situation to be corrected.

A first step in quantifying the limitations of the Gravity Tractor approach is to examine the displacement at Earth impact that would be attained if the baseline Tractor system described in the white paper was to engage Apophis without the aid of a resonant orbit. Figure 21 (analogous to and developed with the same code as was Figure 12)

shows the results of a threat velocity change of 2×10^{-6} m/s impulsively-applied to a *non-resonant* Apophis by the 1-metric-ton Gravity Tractor. Note that a maximum displacements initiated even 10 years before Earth impact (actually earlier than the 2027 mission date) result in displacements of less than 2 millimeters. (The striations in the plot are due to instabilities in the model code, traceable to the use of such a small velocity change.) Unfortunately, if the Gravity Tractor concept is to be applied to non-resonant objects, its mass will have to rise precipitously. Figure 22 shows that a deflection velocity of 0.2 cm/s produces displacements that might be applicable in converting an Earth-skimming impact of a non-resonant Apophis into a miss (albeit with no margin). However, the mass of a Gravity Tractor required to develop this level of velocity change, calculated by the process same described in the white paper, is nearly 1000 metric tons. Some relief is available by taking advantage of the extended temporal engagements available against many non-resonant threats (see Figure 19). Figure 23 shows how required Tractor mass drops considerably when the time of action is extended beyond the baseline 20-day engagement. Note that the circled data point is for the white paper’s baseline Gravity Tractor mass. Note also that while Figure 23 represents threat displacements of small magnitudes that could address only resonant-return threats, the same mass-reduction trend exists for displacements that are large enough to mitigate non-resonant objects. However, Figure 24 shows that to generate displacements useful against non-resonant objects, even when operations are extended out to 80 days, Tractor mass rises dramatically.

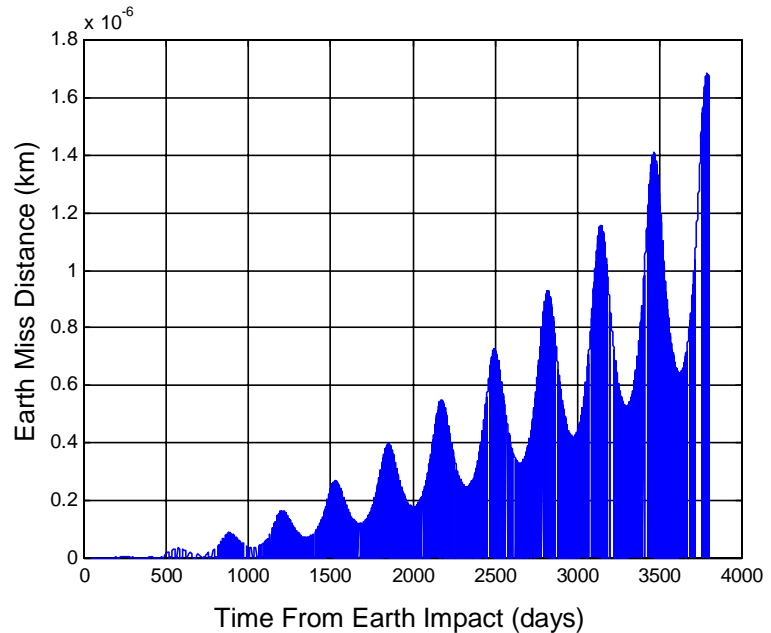


Figure 21. Deflecting Apophis from a Non-Resonant Orbit with the $2\text{-}6$ m/s velocity change described in the Gravity Tractor White Paper.

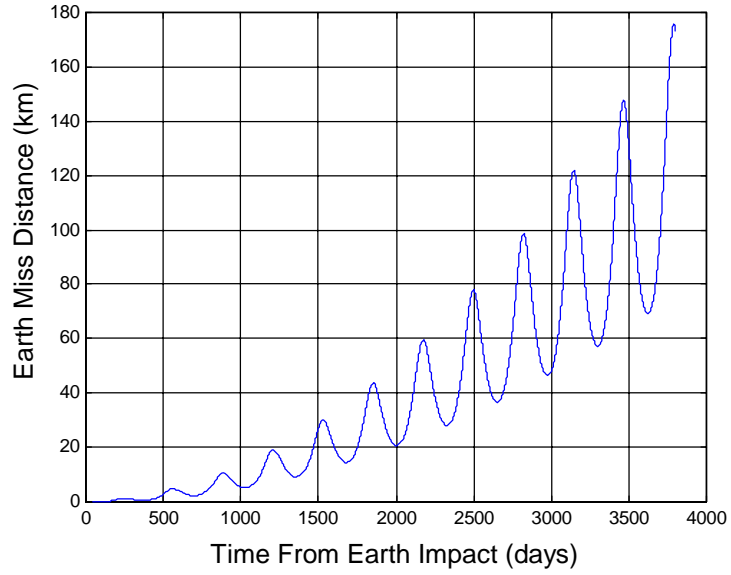


Figure 22. Deflecting Apophis at 0.2 cm/s, three orders of magnitude more than the velocity change described in the Gravity Tractor White Paper.

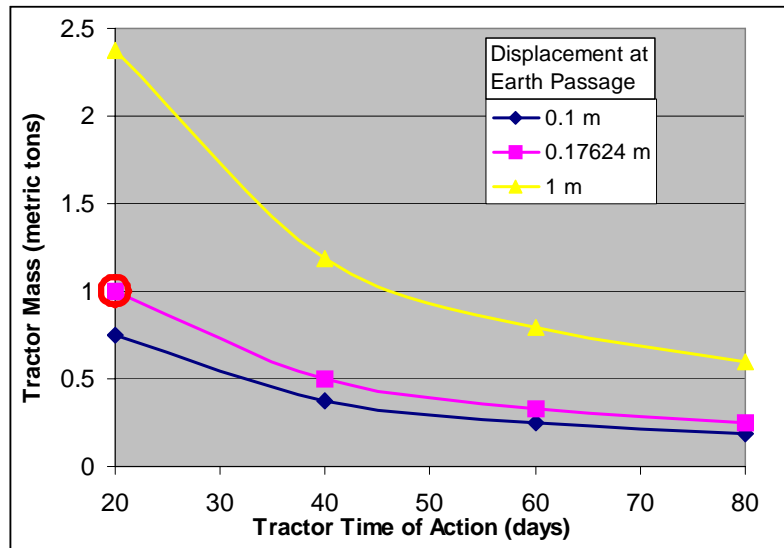


Figure 23. Mass Advantage of Increasing Gravity Tractor Time of Action

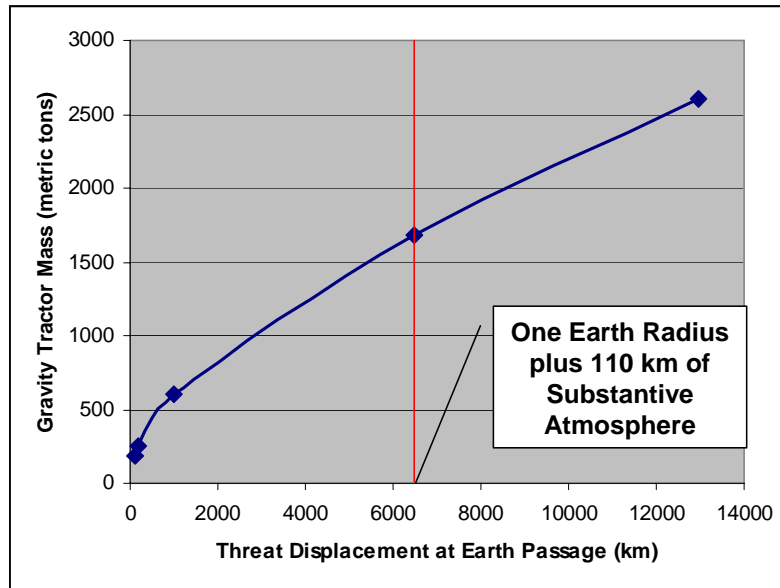


Figure 24. Mass Advantage of Increasing Gravity Tractor Time of Action

¹ Minor Planet Center, Smithsonian Astrophysical Observatory, PHA web site: <http://cfa-www.harvard.edu/iau/lists/Dangerous.html>. (as of 17 July 05).

² Ahrens, T., and Harris, A., "Deflection and Fragmentation of Near-Earth Asteroids," *Hazards Due to Comets and Asteroids*, edited by Tom Gehrels, The University of Arizona Press, Tucson, 1994.

³ Conway, B., "Optimal Low-Thrust Interception of Earth-Crossing Asteroids," *Journal of Guidance, Control, and Dynamics*, Vol. 20, No. 5, pp. 995-1002.

⁴ Park, S., and Ross, M., "Two-Body Optimization for Deflecting Earth-Crossing Asteroids," *Journal of Guidance, Control, and Dynamics*, Vol. 22, No. 3, 1999, pp. 415-420.

⁵ Bate, R., Mueller, D., and White, J., *Fundamentals of Astrodynamics*, Dover Publications, Inc., New York, 1971.

⁶ Prussing, J., and Conway, B., *Orbital Mechanics*, Oxford University Press, New York, 1993.

⁷ Cornell University Library arXiv system, <http://arxiv.org/ftp/physics/papers/0608/0608157.pdf>, publication date unknown

⁸ <http://www.cnn.com/2007/TECH/space/02/19/asteroid.deflector.reut/index.html>